2024-08-09

Modulation of the internal wave regime over a tropical seamount ecosystem by basin-scale oceanographic processes

Ted Robinson *School of Biological and Marine Sciences*

Philip Hosegood *School of Biological and Marine Sciences*

Adam Bolton *School of Biological and Marine Sciences*

Modulation of the internal wave regime over a tropical seamount ecosystem by basin-scale oceanographic processes

Robinson, Ted; Hosegood, Philip; Bolton, Adam

Published in:
Progress in Oceanography

DOI:
10.1016/j.pocean.2024.103323

Publication date:
2024

Document version:
Publisher's PDF, also known as Version of record

Progress in Oceanography 228 (2024) 103323

Contents lists available at ScienceDirect

Progress in Oceanography

journal homepage: www.elsevier.com/locate/pocean

Modulation of the internal wave regime over a tropical seamount ecosystem by basin-scale oceanographic processes

E. Robinson *, P. Hosegood, A. Bolton

University of Plymouth, Drakes Circus, Plymouth PL4 8AA, United Kingdom

ARTICLE INFO

Keywords:
Internal waves
Physical oceanography
Turbulence
Seamounts
Indian ocean dipole
Chagos archipelago

ABSTRACT

Shallow seamounts are becoming increasingly recognised as key habitats for conservation due to their role as biological refuges, particularly throughout oligotrophic oceans. Traditionally, Taylor caps have been invoked as the mechanism driving biomass aggregation over seamounts but emerging evidence based on higher resolution measurements highlights the importance of internal waves (IW) to the local ecosystem. These waves can flush the benthic habitat with cool water from depth and impact on nutrient supply over short time scales through turbulent mixing that may also influence fish behaviour. They are dependent on the regional stratification, however, and thus influenced by planetary-scale variability in oceanographic conditions. We present here detailed observations of the internal wave regime over a shallow seamount, called Sandes, in the central Indian Ocean throughout different phases of the Indian Ocean Dipole (IOD) that modulated the regional stratification. A deep thermocline, caused by the 2019 IOD event precluded internal wave activity over the summit, whereas a thermocline collocated with the summit during 2020 when the IOD reversed polarity resulted in a 30 m amplitude internal tide signal (t ~ 12.5 h). A shallow thermocline, observed during 2022, resulted in propagation of IWs over the summit with less visible internal tide. Harmonic analysis shows the presence of high frequency waves (t ~ 15 min) on both flanks of the seamount during 2020 & 2022, which are likely a result of local shear instability, whereas 2019 shows an asymmetric response, potentially due to the strong background current and suppression of the thermocline beneath the depth of the summit. The potential importance of the waves over the summit to the local ecosystem may be attributed to the elevated turbulence measured at the thermocline during internal wave propagation, with $\varepsilon > 10^{-5}$ W kg-1 routinely observed. Our results highlight the ability of thermocline depth to act as a gating condition for internal wave evolution over the summit. These results show that, whilst the water column exhibits variability at short spatiotemporal scales compared to the frequently cited Taylor cap dynamics, it is also regulated by the wider basin scale processes. Thus, a more integrated approach is needed when assessing these dynamic and environmentally critical habitats to include the effects of physical oceanographic controls across multiple spatiotemporal scales.

1. Introduction

Shallow seamounts are widely recognised as biological hotspots that host thriving ecosystems (Morato et al., 2010). These seamounts are numerous throughout the world's oceans, with recent estimates based on global SRTM v.11 bathymetry placing the total number of seamounts and pinnacles at over 30,000, with approximately 2000 of these extending as shallow as 200 m below the surface, and therefore likely to enter into the euphotic zone (Yesson et al., 2020, 2011). The International Hydrographic Organisation defines a seamount as an elevation over 1000 m (International Hydrographic Organization, 2019), meaning that despite being previously defined as a seamount (Hosegood et al., 2019) Sandes is more physically characteristic of a pinnacle standing only 600 m tall (Harris, 2007; Staudigel et al., 2010). Seamounts and pinnacles have, however, previously been considered largely analogous from an ecosystem and biodiversity perspective (Galbraith et al., 2022), despite the potential for vastly different physical scales, and as such are often studied as a collective.

Due to the low resolution of global bathymetry datasets, the estimated global seamount count is likely to be a significant underestimate and is unlikely to resolve small pinnacles such as those found throughout the tropics. Despite their recognised importance to the marine

* Corresponding author.
E-mail addresses: edward.robinson@plymouth.ac.uk (E. Robinson), phil.hosegood@plymouth.ac.uk (P. Hosegood), adam.bolton@plymouth.ac.uk (A. Bolton).

https://doi.org/10.1016/j.pocean.2024.103323
Received 23 October 2023; Received in revised form 3 August 2024; Accepted 7 August 2024
Available online 9 August 2024

ecosystem, several reviews have highlighted our poor understanding of the dynamical regime that influences, and potentially controls, these habitats despite their abundance throughout the world's oceans (Clark et al., 2012; Lavelle and Mohn, 2010; McClain, 2007; Rowden et al., 2010). Many of these deficiencies can be attributed to the practical challenges surrounding the sampling of these highly localised, subsurface regimes, but also their geographic isolation. Due to these factors conducting observational studies with in-situ observations becomes resource intensive but remains necessary to build a robust characterisation of the dynamic conditions that enable these habitats to host a rich variety of species. Whilst several studies allude to the dynamics surrounding seamounts which may be responsible for the localised biomass aggregation, they are predominantly reliant on coarse scale measurements (e.g.Campanella et al., 2021; Ma et al., 2021; Domokos, 2022). As such they are unlikely to capture data at the temporal scale of the dynamics which are ubiquitous in these energetic environments, nor resolve fine scale spatial variability within ecosystems.

In the absence of widespread, purposeful measurements over seamounts of varying scales, multiple mechanisms have been posited as being responsible for the local increase in biomass at seamounts. Early theories on the dynamics over these seamounts centred on processes which evolve over longer time scales, such as the formation of Taylor caps and the generation of upwelling, although in-situ observations are limited in scope and rarely present irrefutable evidence of persistent upwelling of nutrients (Boehlert and Genin, 1987; Brechner Owens and Hogg, 1980). However, without measurements which can resolve the high frequency processes over the seamount, the isolation of the actual drivers is difficult due to the risk of aliasing in low resolution datasets (Domokos, 2022; Galbraith et al., 2022; Ma et al., 2021), for example inversion of the tidal flow may appear as circular flow in slow sampling datasets.

Whilst the slow geostrophic flows observed over large-scale deep seamounts may be compatible with Taylor cap formation (Campanella et al., 2021; Domokos, 2022), shallow seamounts (in this instance seamounts with summits $<$ 200 m in depth) tend to exhibit a physical regime that is comparatively more energetic at short time scales. These shallow seamounts do not tend to exhibit the slow and steady flow required for the persistence of Taylor caps (Chapman and Haidvogel, 1992; Stevens et al., 2014). Their steeper topography and small summits are likely to result in larger Rossby numbers which are parametrically less compatible with Taylor cap formation, and as Coriolis force plays a key role in Taylor caps initiation, they are also less likely to form in a stable manner near the equator where the Coriolis force is comparatively small (Chapman and Haidvogel, 1992).

Furthermore, at the scale of pinnacles, the short horizontal distances associated with the summit mean that any local upwelling would be rapidly transported away from the summit, producing a signal downstream of the summit resembling the surface wakes formed by the Island Mass Effect (Genin, 2004; Turnewitsch et al., 2016). Recent findings have thus focused on the energetic processes that dominate at these seamounts, such as internal waves, eddies, and turbulence (Dewey et al., 2005; Hosegood et al., 2019; Read and Pollard, 2017; Van Haren et al., 2017).

Internal waves are frequently observed at these steep sloped seamounts (Hosegood et al., 2019; Mohn et al., 2021; Read and Pollard, 2017; Toole et al., 1997; Van Haren et al., 2017) and are capable of vertically advecting cold water from below the mixed layer into the euphotic zone over short timescales. In the Indian Ocean, and equatorial region in general, internal waves are likely to exert the greatest influence on the ecosystem in the upper ocean due to the strong thermocline. The thermocline itself exhibits variability over seasonal timescales (Burns and Subrahmanyam, 2016), which within the archipelago is primarily driven by the monsoon, and over interannual timescales by the Indian Ocean Dipole, one of the major basin scale ocean–atmosphere processes in the Indian Ocean (Diaz et al., 2023; Liu et al., 2022; Robinson et al., 2023).

Internal waves are also capable of transporting and concentrating plankton into patches (Franks, 1995; Franks et al., 2020; Lennert-Cody and Franks, 2002, 1999) directly affecting lower trophic level food source distributions. Seamounts which extend into the photic zone also trap vertically migrating zooplankton during sunrise, when the seamount summit is shallower than the Deep Scattering layer from which zooplankton rise at dusk to prey on phytoplankton near the surface (Cascão et al., 2019). Additionally, the multiple degree temperature variability which internal waves can induce is likely to impact on sensitive benthic coral communities which inhabit these tropical regions (Diaz et al., 2023; Reid et al., 2019; Wyatt et al., 2020).

Here we explore seasonal and interannual variations in the internal wave field at Sandes Seamount (hereafter referred to as Sandes), a shallow pinnacle situated in the Chagos Archipelago in the Central Indian Ocean (Fig. 1). Previous observations have demonstrated the seamount to be an important 'hot-spot' for sharks throughout the region and suggested internal waves may be responsible for aggregating prey (Hosegood et al., 2019).

The summit of Sandes sits at a depth of approximately 70 m, is relatively flat, and 2.2 km along the longest (Southwestern) edge. The flanks of the seamount are steep, with slope angles above 50° and therefore supercritical to internal tides at diurnal and semidiurnal frequencies (Hosegood et al., 2019). Sandes has been the subject of previous studies which have highlighted the potential role of internal waves in promoting biomass aggregation (Hosegood et al., 2019) but focussed on environmental conditions during which the thermocline intersected the seamount summit. In this paper, we present a range of observational evidence to demonstrate the heterogenous impact of internal waves over the seamount, and the modulation of the internal wave regime by basin-scale changes in stratification arising from the influence of the Indian Ocean Dipole. The overall aim of this paper is to elucidate the primary control of internal waves on the biophysical regime over this and similar seamounts alongside their susceptibility to the influence of background changes in water properties and currents.

This paper is structured as follows, firstly the theory relating to internal wave is presented to highlight the pivotal role played by the steep slopes typical of these shallow pinnacles, as well as the background stratification. Secondly the methodology and data collection are detailed, as well as the background meteorological conditions based on regional scale models. We then highlight why Sandes and equivalent features throughout the oceans are unlikely to enable the formation of Taylor caps before presenting evidence of internal wave activity and demonstrating its variability over time. These results are further supported by both frequency domain analysis and quantification of local turbulence and mixing generated by the IW over the seamount summit. Finally, we contextualize these results within the growing body of work focused on high frequency dynamics at seamounts, to expand the understanding of how these short period processes evolve over longer time scales in the presence of variable stratification.

2. Influence of stratification and bathymetric slope on internal wave evolution

The strength of the background stratification dictates the characteristic slope of internal waves and their subsequent generation over, and interaction with, the slopes surrounding seamounts. Additionally, the local buoyancy frequency, $N^2 = g/\rho_0 \delta\rho/\delta z$ where ρ is the in-situ density and g is the gravitational acceleration, acts as the upper boundary for the internal wave frequency, with the local Coriolis frequency, $f = 2\Omega\sin\theta$ where Ω is the Earth's angular velocity and θ is the latitude, being the lower limit.

At steep sloped seamounts like Sandes the oscillatory flow over the summit with the tide can result in the generation of lee waves on the downstream flank. The regime within which these waves fall is governed by two key parameters. The first parameter is the intrinsic frequency, $U_0 k$, where U_0 is the flow velocity and k is the horizontal wavenumber,

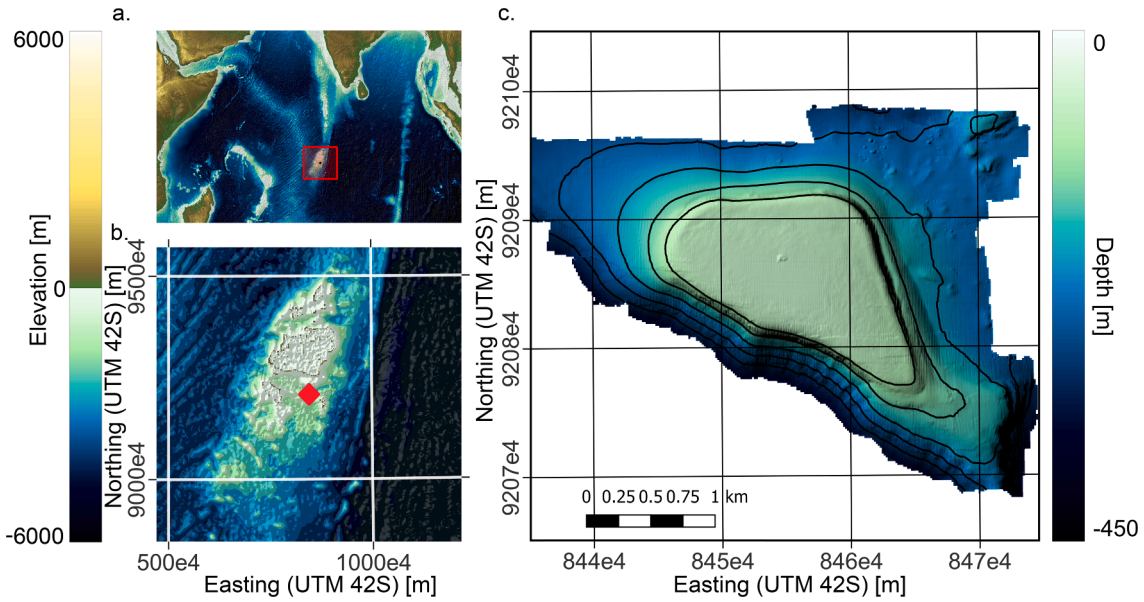

Fig. 1. Chart of the (a) Indian Ocean, and (b) Chagos Archipelago based of the 2022 GEBCO grid (GEBCO Compilation Group (2023) GEBCO 2023 Grid (https://doi.org/10.5285/f98b053b-0cbc-6c23-e053-6c86abc0af7b)) (c) High resolution multibeam bathymetry of Sandes Seamount, showing steep slopes on each of the flanks (collected during the November 2019 expedition). Contours at 50 m intervals.

and the lee-wave Froude number, $Fr^{-1} = N\ h_0/U_0$, where h_0 is the height of the obstruction relative to the surrounding seafloor (Klymak et al., 2010; Legg, 2021), and the formation of non-linear internal waves is expected when $Fr^{-1} > 1$. Comprehensive reviews of lee wave regimes and internal tide generation can be found in Legg (2021), and Garrett and Kunze (2007), but in summary the scenarios presented herein cover moderate flows and strong stratification, are likely to result in the generation of strongly nonlinear internal lee waves (Klymak et al., 2010) given the approximate Fr^{-1} value over the summit of 6 based on $N = 2.5 \times 10^{-3}$m, $h_0 = 600$, and $U_0 = 0.25$.

The generation of internal tides (which are internal waves forced at tidal frequencies) is possible at a wide range of slopes, with ridge like features generally being more effective generators than isolated seamounts and islands (Holloway and Merrifield, 1999). Recent observations have shown that internal tides are almost ubiquitous throughout the world's oceans (Müller et al., 2012; Zhao, 2018). Satellite altimetry shows the presence of internal tides along the Chagos-Laccadive ridge, on which Sandes is situated, and in particular highlights the central Indian Ocean as a 'hotspot' for diurnal internal tides (Shriver et al., 2012).

The interactions between incoming internal waves and topography are governed by the relationship between the slope of the internal wave, defined as $\gamma_{IW} = \left[\left((\omega^2 - f^2)/(N^2 - \omega^2)\right)\right]^{1/2}$, where ω is the wave forcing frequency (LeBlond and Mysak, 1978), and the slope of the seabed γ_{BED}. For incoming waves interacting with topography, subcritical slopes ($\gamma_{BED}/\gamma_{IW} < 1$) will result in upslope reflection of the wave, supercritical slopes ($\gamma_{BED}/\gamma_{IW} > 1$) result in partial offshore reflection of the wave, and critical slopes ($\gamma_{BED}/\gamma_{IW} = 1$) result in the decomposition and breaking of the wave in a nonlinear fashion (Hall et al., 2013).

At supercritical slopes, mechanisms for inducing turbulence and mixing include strong wave breaking activity (van Haren, 2023), and the generation of upslope propagating boluses (Lamb, 2014). The incident reflection of the internal tide has also been linked to elevated turbulence at these steep slopes (Hamann et al., 2020). These localised areas of enhanced mixing due to turbulence may be responsible for driving the increase in high trophic level aggregation which is seen over the slopes at some seamounts (Campanella et al., 2021).

With the study site situated at ~−7° N, the frequency band in which internal wave activity is sustainable spans a range of ~97 h – 130 s (f – N_{max}). Due to the strong stratification, internal waves forced by the M_2 tide have shallow slopes relative to the local bathymetry with typical slopes <2° relative to the >50° seamount topography slope. A comparison of the local wave slope based on the stratification profile against the local bathymetry in both November 2019 and March 2020 shows that, apart from the plateau of the summit, the seamount is almost exclusively supercritical (Fig. 2) making the conversion of the local tidal energy into internal waves ineffective across much of the seamount flank.

3. Methodology

Data were collected during three research cruises to the Chagos archipelago in November 2019, March 2020, and March 2022. During each cruise, several near-bed, and subsurface taut line moorings were deployed over the summit and flanks of Sandes, to resolve with high temporal and vertical resolution the evolution of internal waves over a transect spanning the summit. Additionally, profiling measurements were made with a RBR Maestro CTD in 2019 and 2020, and with a combination of RBR Maestro CTD and a Sea & Sun MSS 90 multiparameter profiler for turbulence measurements during 2022.

3.1. In-situ observations: Moored measurements

Moorings were deployed along a transect aligned, approximately, from east to west to be in line with the semi-major axis of the M_2 tidal constituent (Hosegood et al., 2019) and the prevailing westwards South Equatorial Current (SEC) (Fig. 3). The overall goal of the mooring array was to capture the evolution of internal waves over and around the summit because of the interaction between tidal and background currents, and the seamount flanks. Details of the moorings are presented in Table 1.

All moorings were subsurface, taut line moorings equipped with a variety of acoustic-Doppler current profilers (ADCP) and temperature sensors. RDI Workhorse Monitor, Nortek Signature, and Nortek Aquadopp ADCPs were deployed, alongside RBR Solo^{3}T and SBE 56 temperature sensors, as well as Starmon TD, and RBR Concerto CTD sensors for depth information. The mooring transects in 2019 and 2022 extended from 150 m depth either side of the summit, thereby capturing the behaviour of the thermocline even during the exceptional conditions

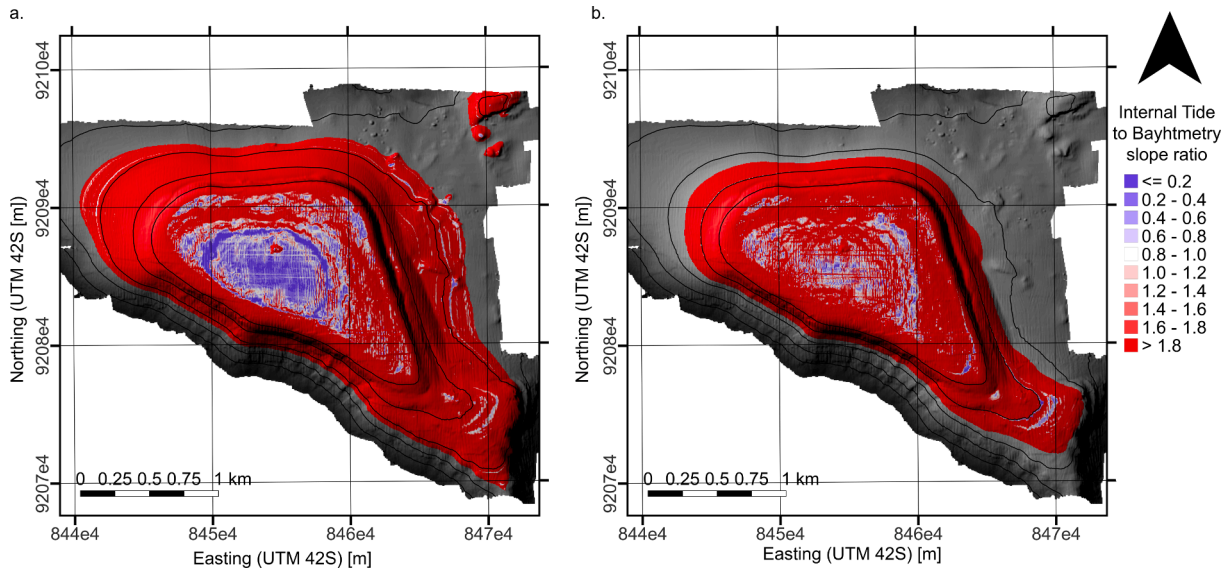

Fig. 2. Map of Sandes showing sub, and supercritical areas based on the slope of an M_2 forced internal tide in (a) November 2019 and (b) March 2022. Values <1 denote subcriticality, and >1 supercriticality. This demonstrates the steep slopes of Sandes relative to the internal tide as the flanks are almost entirely supercritical. Contours at 50 m intervals.

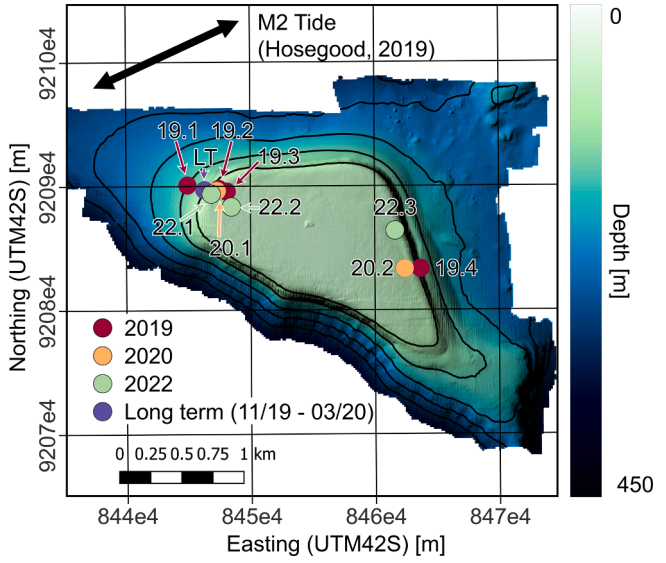

Fig. 3. Sandes with mooring locations overlaid showing the Northwest – Southeast alignment in line with the previously reported tidal flow. Contours at 50 m intervals. Annotated with M2 major axis as reported in Hosegood (2019).

of 2019. The 2020 transect had a reduced extent and only covered up to 90 m on the flanks of the summit.

A long-term mooring consisting of a Nortek Signature 500 ADCP was deployed on the western flank of Sandes between November 2019 and March 2020 for 106 days, providing velocity profiles at 10-minute intervals with a 2 m vertical resolution.

Moored ADCP data were filtered to remove data with correlation values < 40 % due to the clear-water conditions reducing correlation. In March 2022 the Nortek Signature 500 kHz ADCP sampled with velocity burst sampling at 1 Hz with a 0.5 m vertical bin size, and was bin averaged to 30 s samples for analysis using Ocean Contour. Echosounder data were collected using the central beam of the ADCP at 1 Hz with a 6 mm vertical resolution and were bin averaged to an 18 mm vertical and 10 s temporal resolution for analysis, a logarithmic decay correction was applied to normalise the signal gain over the water column.

Table 1
Mooring timings and structure overview.

Mooring ID	Depth (m)	Start Time	End Time	Duration (Days)	Type
19.1	155	14/11/2019 17:51	23/11/2019 17:00	9.0	ADCP+Thermistor
19.2	80	15/11/2019 08:10	23/11/2019 18:00	8.4	ADCP+Thermistor
19.3	79	14/11/2019 13:50	22/11/2019 11:55	7.9	ADCP+Thermistor
19.4	125	15/11/2019 09:30	24/11/2019 06:43	8.9	ADCP+Thermistor
20.1	80	07/03/2020 18:38	18/03/2020 07:20	10.5	ADCP+Thermistor
20.2	90	07/03/2020 17:44	18/03/2020 08:14	10.6	ADCP+Thermistor
22.1	94	15/03/2022 14:22	28/03/2022 08:30	12.8	ADCP+Thermistor
22.2	71	19/03/2022 17:14	28/03/2022 09:10	8.7	ADCP
22.3	84	15/03/2022 12:28	28/03/2022 08:06	12.8	ADCP+Thermistor
LT	104	02/12/2019 18:30	18/03/2020 06:50	106.5	ADCP

The thermistors on all moorings logged at 1 Hz on a common time frame and were cleaned with a 5-point 1-deviation Hampel filter in the time domain.

3.2. *Ship-based measurements: Conductivity-Temperature-Depth (CTD), turbulence, and vessel mounted ADCP (VMADCP)*

Vertical CTD profiles were taken at irregular intervals during 2019 and 2020 to characterise the background stratification. Buoyancy

frequency values from CTD profiles were calculated based on 0.5 m bin averaged upcast data, with an initial sample rate of 12 Hz. Resulting data were further processed with a 5-point running mean window to reduce the impact of sensor noise.

During 2022, three complete transects were conducted along the mooring array to measure standard CTD parameters and turbulence properties using a Sea and Sun MSS90 profiles with twin shear probes, sampling at 1024 Hz in a free-falling configuration. Between 9 and 11 stations were sampled and the transects were completed with a period of <2.5 h, enabling the results to be viewed as a quasi-instantaneous realisation of the cross-summit properties, however it is important to note that whilst it forms a small subset of the 12.5 h semi-diurnal tide, there will still be some tidal evolution present over the course of a transect. Dissipation rates of turbulent kinetic energy (TKE, ε), were estimated according to Oakey (1982):

$$\varepsilon = 7.5\nu\langle(\partial u'/\partial z)^2\rangle \quad (1)$$

where ν is the kinematic viscosity, and $\langle(\partial u'/\partial z)^2\rangle$ is the variance in gradient of horizontal shear fluctuations over the vertical profile. The measurements of TKE from each shear probe were then averaged together to give a single profile.

A Nortek Signature 100 VMADCP was used to collect repeat underway transects of current velocity and acoustic echo amplitude over the summit. Transects were repeated in a bowtie form over a 24-hour period. Velocity corrections were provided by a dual antenna GNSS system, and motion corrections by the internal AHRS on the ADCP. Validation of the offsets was performed in the Nortek Signature VM Review and averaged over 3 bowtie transects. VMADCP data were cleaned with a 5-point, 1 deviation Hampel Filter, and a 3-point moving mean.

Susceptibility of the water column to overturning and mixing through shear instability was estimated using the Richardson number, $Ri = N^2/S^2$, where $S^2 = (\delta u/\delta z)^2 + (\delta v/\delta z)^2$ where u and v are eastward and northward velocities respectively. Values below the critical threshold of 0.25 indicate a water column that is unstably stratified and susceptible to overturning.

3.3. Indian ocean dipole index

To identify the influence of basin-scale changes in stratification on the internal wave regime, the state of the IOD was evaluated using the NOAA Ocean Observations Panel for Climate Dipole Mode Index (DMI) dataset. The DMI is calculated based on the anomalous sea surface temperature (SST) gradient between the western equatorial Indian Ocean, and the south-eastern equatorial Indian Ocean as defined by Saji et al. (1999) with a climatology based on 1981–2010 (NOAA, 2023).

3.4. Argo data

Argo data is presented from float & profile ID 2902290_021, chosen for its relative proximity to the archipelago at the time of our measurements in 2020. Data were upscaled via linear interpolation to match the 0.5 m resolution of the CTD data. These data are only used to provide context when comparing stratification states (Fig. 5) and are not used in any further calculations.

4. Results

4.1. Background conditions, tidal dynamics, and variability through monsoonal and IOD driven thermocline evolution

During late 2019, one of the most extreme positive IOD events on record caused a deepening of the thermocline over the archipelago and the establishment of elevated and sustained westward currents. An anomalous surface layer nearly 100 m thick was created and which prohibited the generation and propagation of internal waves over the summit of Sandes (Du et al., 2020; Lu and Ren, 2020). During subsequent months, the IOD relaxed into a more typical state, enabling the thermocline to recover to standard depths of ~ 60 m and supporting internal waves over the summit of Sandes.

In this paper, we present observations from three stratification states during which research cruises were conducted to monitor the impact of internal waves over a shallow seamount: Deep (100 m) in November 2019, Intermediate (70 m) in March 2020, and Shallow (40 m) in March 2022. November 2019 followed a record high IOD index of 3.1, March 2020 followed a brief and mild negative IOD with a peak index of −0.78, and March 2022 followed an extended ~5-month period of negative IOD with a mean index of −0.45 between October 2021 and March 2022 (Fig. 4).

Modelling studies have shown that the positive 2019 IOD event generated exceptionally deep surface mixed layers (Lu and Ren, 2020). In-situ CTD profiles taken near the summit of Sandes confirm that over the period of the cruises, stratification varied considerably (Fig. 5). The upper edge of the thermocline (taken here as the 28 °C isotherm) seen in CTD profiles was located at 95 m in November 2019, 70 m in March 2020 and 45 m in March 2022. Peak N^2 was observed at 107 m depth in November 2019 ($N^2 = 2.3 \times 10^{-3}$) and at 48 m in March 2022 ($N^2 = 2.6 \times 10^{-3}$). An estimate of the corresponding value in 2020 was made using the deepest CTD profile and ARGO data, resulting in the peak stratification at ~ 85 m.

A comparison of in-situ data from moorings on the western summit of Sandes during each period (<100 m location difference between the deployments) reveals the impact of the background stratification on the thermal regime (Fig. 6). November 2019 shows a summit inundated with high temperature (>29 °C) surface characteristic water, whereas March 2020 shows water ~27.5 °C over the summit of the seamount at ~ 80 m with additional periodic cooling observed. During March 2022, the thermocline was located above the summit, at 48 m depth, with cooler water from below the thermocline continuously present over the summit. This results in a 6.2 °C change in mean temperature at 70 m depth (the shallowest depth over the summit) between 2019 and 2022. Between 16/11/19–23/11/19 the summit experienced a mean temperature of 28.8 °C compared to 22.6 °C between 16/03/22–23/03/22.

Due to the prominent role of the barotropic tide in forcing internal waves, attempts were made to isolate the dominant tidal constituents, along with their variability over the seamount. Velocity based tidal decompositions at Sandes fail to resolve specific components due to the presumed strong phase-locked baroclinic activity arising from local generation over the summit. However, decomposition using long term pressure observations shows that the M_2 tide is the primary energy contributor at 73 %, compared to 20 % for the S_2 tide, and only 3 % for the K_1 tide (Fig. 7).

4.2. Susceptibility of Taylor cap formation over Sandes

To assess the likelihood of Taylor cap formation over Sandes, a parametric analysis was conducted and the values compared to thresholds for Taylor cap feasibility as presented in Chapman and Haidvogel (1992).

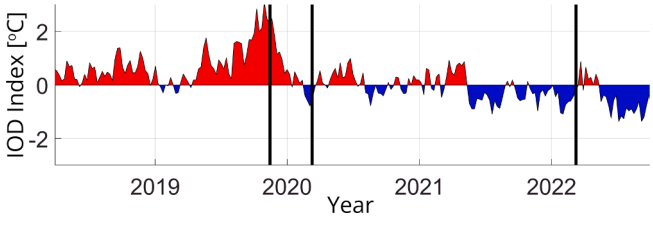

Fig. 4. IOD Index for the period covering the data collection, with the three periods marked showing the differing IOD conditions which preceded each trip.

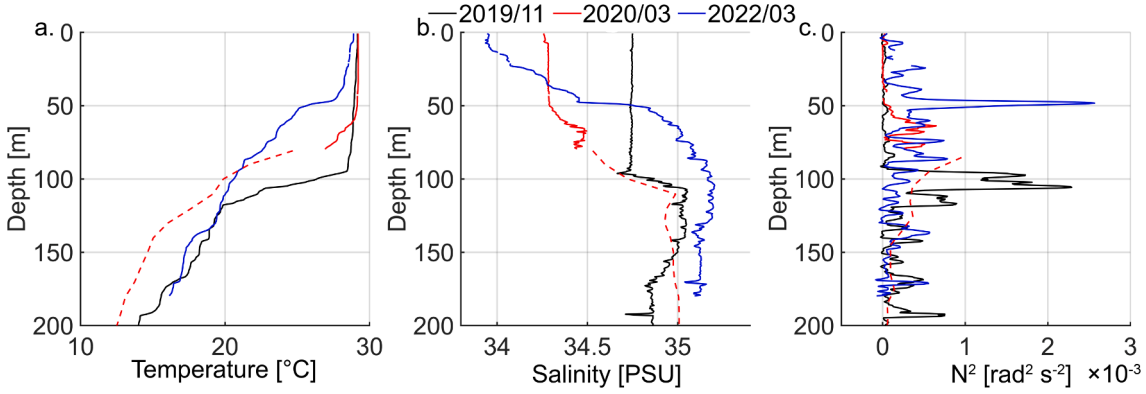

Fig. 5. (a) Temperature, (b) salinity, and (c) buoyancy frequency squared (N^2), from CTD profiles in the Chagos Archipelago in November 2019, March 2020, and March 2022. N^2 values show the evolving depth of maximum stratification due to the movement of the thermocline. Data below 80 m in March 2020 is from ARGO profile 2902290_021 and indicated by the dashed line.

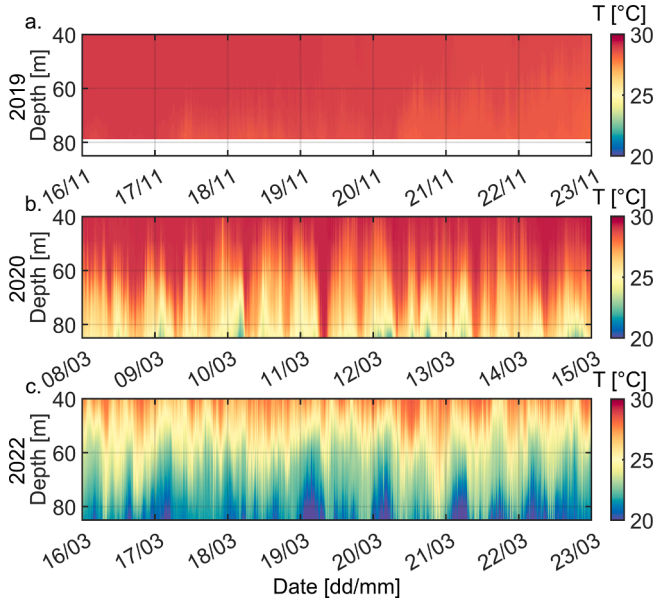

Fig. 6. Thermistor data from the western summit of Sandes from (a) November 2019, (b) March 2020, and (c) March 2022, showing the impacts of differing thermocline depth in the stratification and regime over the summit.

The Burger Number ($B=NH/fL$) provides a measure of the strength of vertical stratification against the horizonal where H is the water depth away from the seamount, and L is the horizontal scale of the seamount. In the case of Sandes $f = 1.77 \times 10^{-5}$ s^{-1}, L ~ 2000 m, H = 600 m, and N is of the order 1×10^{-2} rad s^{-1}. This gives B = 16.9, indicative of a stratification dominated regime where any Taylor cap would be trapped near the bed.

The Rossby number ($R=U/fL$) is a ratio of the horizonal and rotational velocities. The maximum instantaneous velocities observed over Sandes were ~0.5 m/s, but average velocities over the summit were lower at 0.16 m/s. Therefore Sandes experiences an average R of 4.5 and a peak R > 14.1, both of which are far above the threshold for Taylor cap formation of 0.4 under a stratified regime (Chapman and Haidvogel, 1992; Huppert, 1975). Note that the low values of f near the equator will render the formation of Taylor caps unlikely throughout the tropics. Combined these factors render Taylor cap formation over Sandes almost entirely impossible.

Whilst these metrics are useful for assessing the general feasibility of Taylor cap formation over the seamount, they represent a static calculation under one set of conditions and do not account for any variability over the seamount, which may provide transient conditions more compatible with Taylor cap formation. Using in-situ data is therefore necessary to detect the presence of a Taylor cap over the seamount.

CTD transects over the summit in 2022 when the thermocline was midway between the surface and summit show no clear doming of the isotherms as would be associated with the presence of a Taylor cap; instead, the variations in isotherm depth are irregular over the summit, and indicative of higher frequency perturbations (Fig. 8).

In addition to varying over the long term with changes to the stratification, the dynamics over the seamount vary with the tidal cycle. Fig. 9 shows three transects which ran east to west over the summit in 2022, each with a duration approximately 1.5 h. The velocities over the summit reach up to 0.5 m/s, and the flow direction shows the presence of a 2–3-layer system depending on the state of the tide, with 180° contraflow layers seen over the summit in all three transects. Transect one shows westward flow at the surface with eastward flow near the bed on the ebb tide, transect two captures a transitional phase in flow direction following low-water slack, and transect three shows the inverse of transect one on the flood tide, with eastward flow at the surface and westward flow at the bed. Whilst a multi-layered system exists over the summit, there is no evidence to suggest any rotational flow as would be associated with Taylor cap formation.

All three transects show localised turbulence of the magnitude 1×10^{-5} W kg^{-1}, which is far above the background values near Sandes of $1 \times 10^{-10} - 1 \times 10^{-8}$ W kg^{-1} with the highest values in all three transects observed close to the downstream (at the depth of the summit) flank of the seamount.

4.3. *Variability in internal wave energy during differing background stratifications*

To quantify differences in internal wave induced variability between stratification states, power spectral density (PSD) from 70 m depth (the shallowest depth over the summit), on both the east and West flanks are shown in Fig. 10.

The lack of thermal variability at 70 m due to the deep thermocline in November 2019 is clearly visible relative to 2020 and 2022 in the reduced powers seen across the spectrum up to N_{max}. There is a marked difference in the spectra between East and West in November 2019, with a maximum difference of 10 dB W^{-1} Hz^{-1} higher power within the 10–100 cpd waveband on the upstream (East) flank, which is within the frequencies range of internal wave activity. During this period there was a strong westwards background current which may be partly responsible for this asymmetry due to limited flow direction inversion during this period. This difference may be indicative of lee wave formation, where the upstream isotherm is elevated, and the downstream depressed, with the persistent background current preventing the release and rebound of

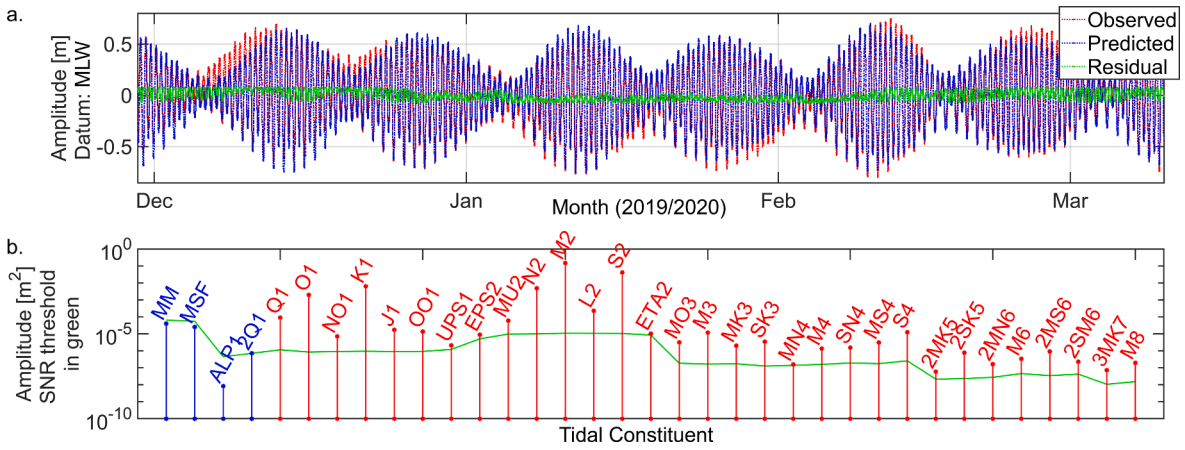

Fig. 7. (a) Observed tidal height (relative to mean water level), and reconstruction based on harmonic decomposition. (b) Tidal components from decomposition, constituents in red are over the snr threshold for resolution (shown in green). m_2 and S_2 components are the core contributors to the total tidal energy. Full definitions of each harmonic can be found in NOAA Special Publication NOS CO-OPS 3 (Parker, 2007). (For interpretation of the references to colour in this figure legend, the reader is referred to the web version of this article.)

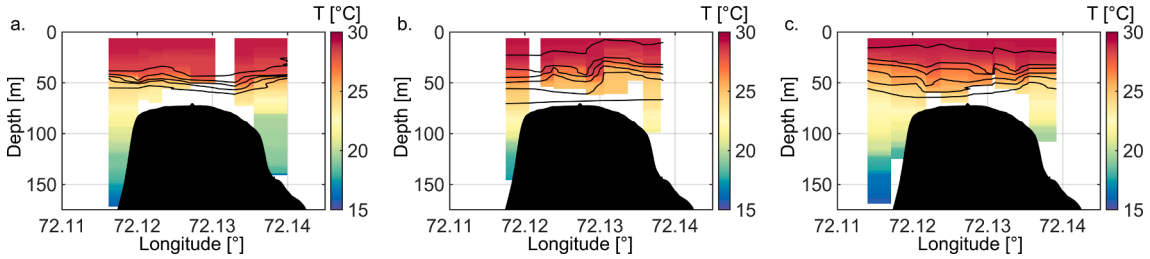

Fig. 8. 1° spaced isotherms [24–28 °C] from MSS transects in March 2022 over the summit of Sandes. There is no visible, persistent doming of the isotherms over the summit span as associated with Taylor caps, but instead multiple perturbations are seen over the summit that indicate the presence of shorter period vertical excursions of the thermocline over the sampling duration.

isotherms which occurs under more typical circumstances.

By averaging data relative to phase of the tide over the same 7 days, the low frequency variability (in this case likely associated with an internal tide) is isolated (Fig. 11). No tidal variability in temperature is seen in November 2019 due to the summit being within the surface mixed layer but March 2020 and 2022 both show an internal tidal signal. The internal tidal signal is strongest in March 2020, with an amplitude of 12 m in the east, and >15 m in the west. In March 2022, the internal tide has a reduced amplitude of 5 m.

As well as the internal tide, high frequency internal waves can be seen within the thermistor chain data in March 2020 and 2022 (Fig. 12) with periods between 5 and 20 mins. In 2020 where the thermocline is coincident with the summit, the tidal perturbations have magnitudes of up to 45 m, whilst the high frequency waves are smaller and predominantly of 5–10 m amplitude. In 2022 the amplitude of the internal tidal signal is reduced with a 21 m maximum observed amplitude; however, the amplitude of the high frequency waves is not distinguishably different from those observed in 2020. In 2022 high frequency internal waves of both elevation and depression polarities are observed, which may be due to the proximity of the stratification (at 50 m depth) to the inflection point, where the thicker layer of the water column changes from being below to above the stratification.

4.4. Internal wave evolution and turbulence generation

During March 2022, turbulence profiles were taken over the seamount. A TKE profile taken at the same location as a moored ADCP shows that the strongest turbulence occurs at the upper interface of the internal waves which corresponds to the base of the surface mixed layer (Fig. 13). At this depth, which is the consistent vertical position of peak TKE associated with the internal waves, $\varepsilon > 10^{-5}$ W kg^{-1}, which is several orders of magnitude larger than background values over the summit of $<10^{-9}$ W kg^{-1}.

The impacts of internal waves can be highly localised, both spatially and temporally. The echo amplitude from the vessel mounted ADCP during the 24-hour repeat surveys over the summit serves as a visual proxy for the depth of stratification (based on an increased concentration of scatterers seen at the thermocline). Direct microstructure turbulence measurements further verifies that these internal wave events are responsible for localised patches of elevated turbulence in proximity to the seamount (Fig. 14).

The VMADCP data shows ~20 m variability in the elevation of the mixed layer base over the summit (Fig. 14a), which is also seen as variation of the thermocline depth in the temperature profiles (Fig. 14g, f) and is consistent with internal wave activity. This layer is consistently characterised by elevated turbulence seen over the summit in 2022 with $\varepsilon > 10^{-5}$ W kg^{-1}. The variability in turbulence over the summit further supports the idea that these spikes in turbulence are associated with internal waves propagating over the summit. In addition to the discrete spikes in turbulence seen in the profiles over the summit which are coincident with the thermocline at ~50 m depth (Fig. 14 c–h) the deeper water profile to the west of the seamount (Fig. 14 b) which was the upstream side of the seamount at the time of the profile, still exhibits ε of 10^{-5} W kg^{-1} in the 100–150 m depth range while in proximity to tho topography.

Richardson number and TKE dissipation rates show little definitive relationship, although larger shear values are correlated with lower Ri values over the seamount, demonstrating that shear plays a controlling role in producing instability instead of reduced stratification strength (Fig. 15a). The distribution of these high shear values is also centred

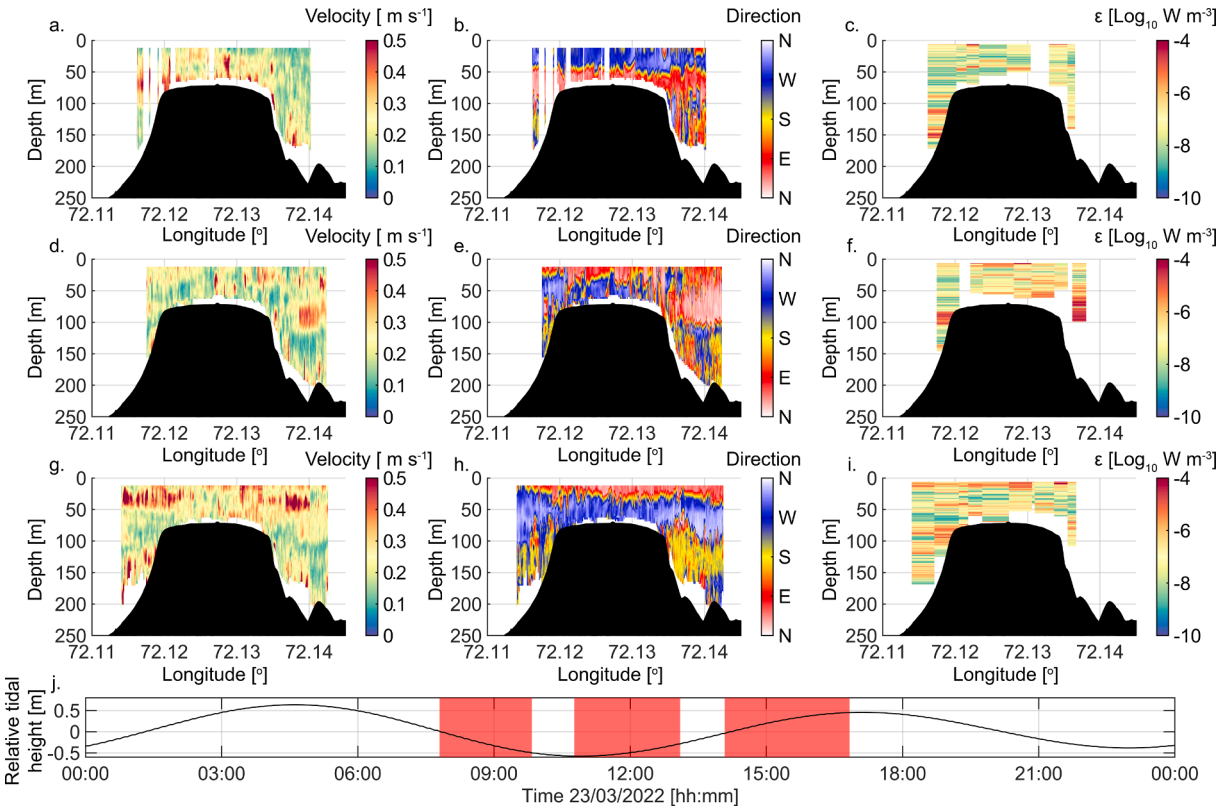

Fig. 9. MSS and VMADCP transects over Sandes in March 2022. Transect 1 (a–c) is the same period shown in Fig. 14 and is on an ebb tide, Transect 2 (d–f) is just following low-water slack, and Transect 3 (g–i) is on the flood tide. Panel j. shows the transects relative to the tidal cycle. Running direction was East to West. Transect 1 covers 07:48–09:50, transect 2 covers 10:46–13:06, and transect 3 covers 14:05–16:30.

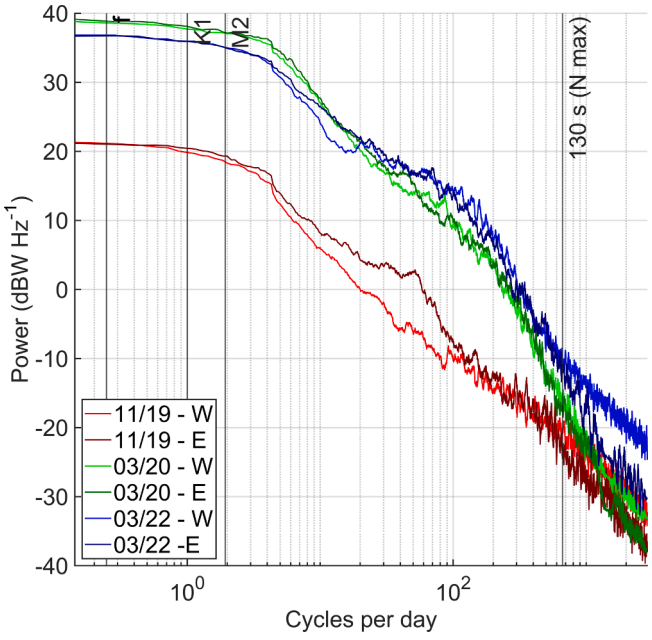

Fig. 10. PSD from 7 days of temperature data from 70 m depth at East and West Sandes moorings in (red) November 2019, (green) March 2020, and (blue) March 2022. Whilst East and West in all three periods are similar, the relative lack of thermal variability in November 2019 is clear. Additionally, the non-standard roll off in 2020 and 2022 shows the presence of internal wave activity in the band between 10 CPD and N. Data are filtered with a 512 running point average to improve visual clarity in the >10 cpd frequency range. (For interpretation of the references to colour in this figure legend, the reader is referred to the web version of this article.)

around the upper elevation of the thermocline in the presence of waves of elevation at 40 m, rather than the 50 m resting depth of the thermocline implying that the internal waves play a key role in enhancing the shear instability and mixing over the seamount (Fig. 15b).

5. Discussion

Shallow seamounts which extend into the photic zone are increasingly recognised as being important biological refuges (Watling and Auster, 2017), but their small-scale presents multiple challenges when diagnosing the dynamics responsible for creating a thriving ecosystem. Their small spatial scales are difficult to resolve, both in terms of detecting them through remote bathymetry and determining their dynamical regime through coarse scale models. Therefore, despite their high ecological value, they remain understudied. This is especially true for those summits such as Sandes which may be better classified as pinnacles to distinguish them from the larger, deeper seamounts that have traditionally received attention.

Sandes shows no visible doming of the isotherms which would be associated with the formation of Taylor caps, and the cross-summit flows are of a sufficient magnitude to rapidly destroy any circulating structures which may form over the summit (Chapman and Haidvogel, 1992). Additionally, the velocities observed over the summit would result in any locally generated productivity being rapidly swept downstream (Genin, 2004; Pitcher et al., 2008). Sandes is not a unique specimen, and many characteristics of the physical regime which we describe are a common feature among these steep tropical pinnacles (Galbraith et al., 2022), as well as at larger tropical seamounts for which the local Coriolis force is small and which still extend into the photic zone (Read and Pollard, 2017). Therefore, there is strong merit in moving away from the hypothesis of Taylor caps being responsible for the increased productivity at these energetic sites, and at small-scale seamounts in general

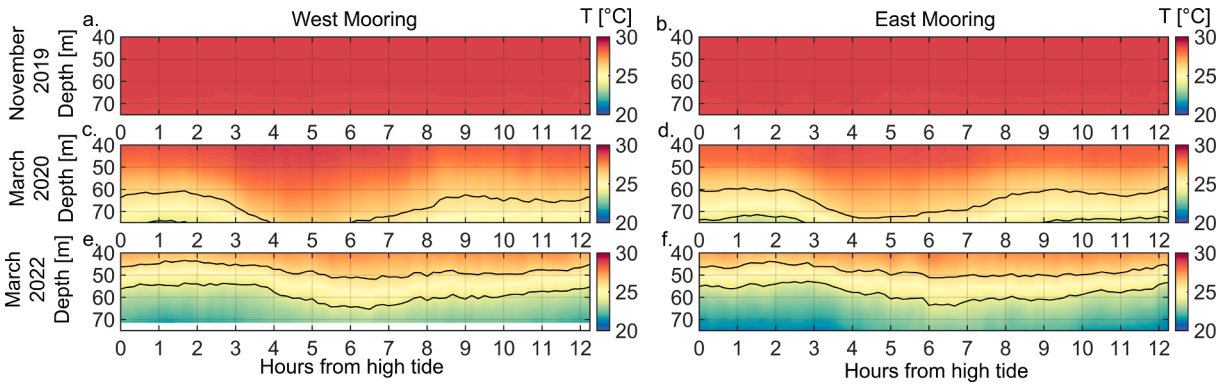

Fig. 11. Duration matched thermistor data time binned against tidal cycle in 10-minute intervals. (a) 2019 shows little internal activity. Clearly visible in (b) March 2020 is the internal tidal signal, which is diminished over the East flank relative to the West. (c) March 2022 shows a reduced amplitude internal tide, implying that interaction with the topography in March 2020 plays a role in modulating the amplitude due to the short spatial separation of the moorings limiting the impact of other external differentiating factors.

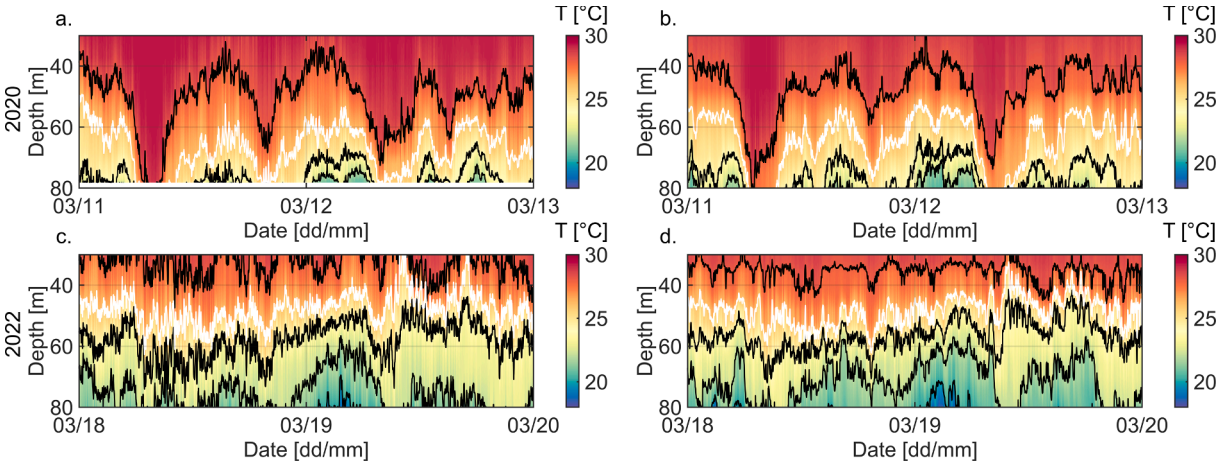

Fig. 12. High frequency thermistor mix of elevation and depression internal data from March 2020 (a, b) and 2022 (c, d) West, (a, c) and West (b, d) of Sandes. The large internal tide in 2020, and the waves in 2022 are both clearly visible.

which have similar characteristics.

At tidal and subtidal frequencies Sandes is instead highly energetic with internal wave activity. Combined with the short horizontal scale of the seamount, this leads to internal waves over the summit on both phases of the tide when the stratification is above the summit depth, rendering them a more ubiquitous feature in shallow stratification than seen in studies at topographically obstructed shelfs and banks (e.g. van Haren et al., 2019). Given the supercriticality of the slope at Sandes, the local generation of internal waves is possible in all three stratification scenarios, but the lack of near-critical slopes coincident with the peak stratification does mean this will be less effective than at critical slopes. The supercriticality does, however, introduce the possibility of localised turbulence near the flanks through several previously documented processes such as breaking and reflection of the internal tide, and the development of turbulent boluses on the downstream flank of the seamount (Lamb, 2014; van Haren, 2023). Whilst Sandes shows an internal wave regime with some similarity to those presented by Stevens et al., (2014), the impacts of a strong background current in November 2019 result in elevated energy in the internal wave band on the upstream flank of the seamount in the case of deep stratification below the seamount summit, as opposed to downstream of the summit.

The presence of high frequency waves increases the likelihood of mixing through shear instability, elevating the levels of mixing over the seamount and its flanks and potentially increasing the availability of nutrients to the euphotic zone through turbulent entrainment. The values of turbulence we record in association with high frequency internal waves are far above the ocean background values (Tanaka et al., 2021). The layers of elevated turbulence seen in the profiles are very thin, being collocated with the interface of the internal wave in strong background stratification, and whilst there is a lack of Ri-TKE relationship, this is likely to be a result of the coarse vertical resolution of the VMADCP data, as well as time-based averaging reducing the shear observed in the VMADCP. Overall, the dynamic processes present are a marked departure from the slow steady state upwelling to which the enhanced productivity at seamounts is often attributed.

The local dynamical regime is set in strong, but variable, background stratification. This stratification is controlled by both the monsoon and the IOD (Liu et al., 2022), and under sufficiently strong conditions the thermocline depth can act as a gating condition for internal wave activity over the summit. This then suggests that a short-term approach, purely classifying these sites based on presence-absence over limited time periods, carries a very real risk of excluding sites which under different background forcing may be far more active. While studies on the seasonality of seamount ecosystems and physical oceanographic at numerous sites have been conducted (Arístegui et al., 2009; Mouriño et al., 2001; Santos et al., 2013; Trasviña-Castro et al., 2003), the combination of high resolution with long timescales remains comparatively unexplored.

Internal wave – topography interactions are highly sensitive to both the background stratification (Stashchuk and Vlasenko, 2021), the geometry of the topography (Johnston and Merrifield, 2003), and even the proximity of other nearby topographic features (Zhang et al., 2017) that

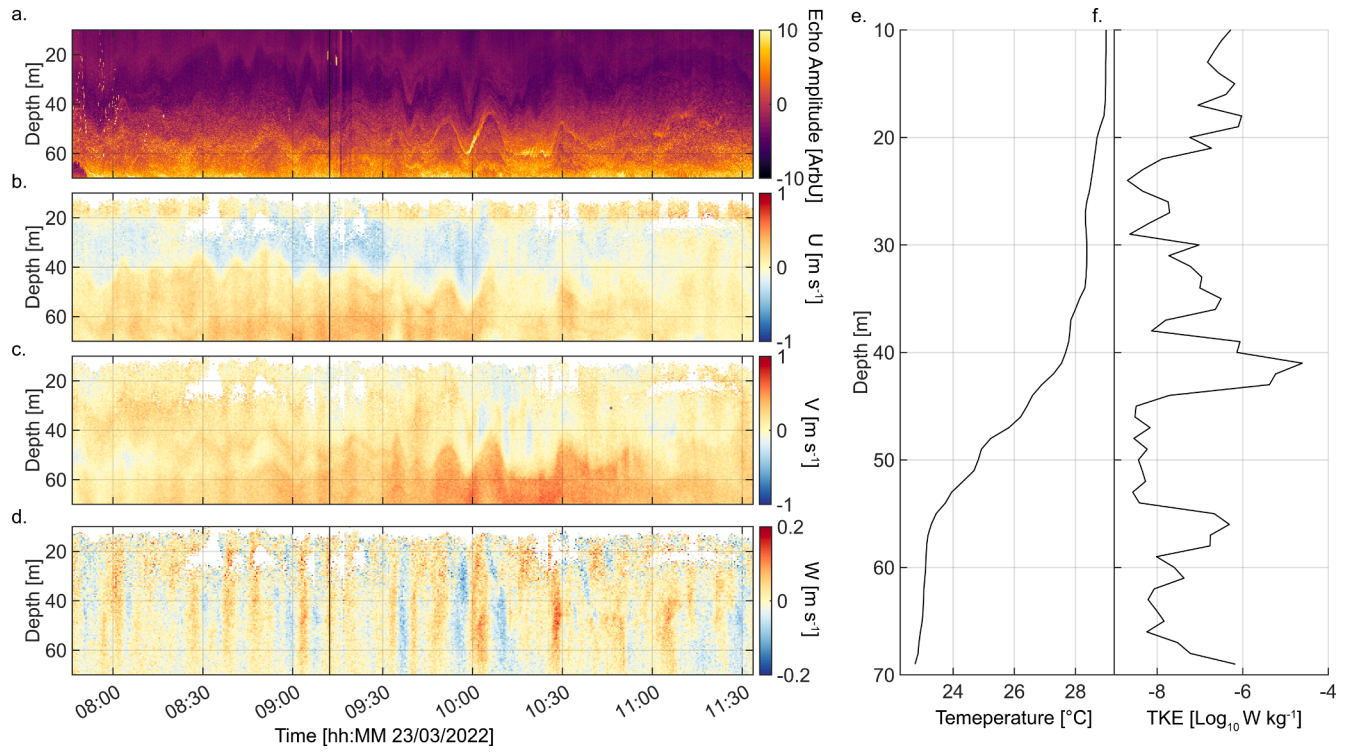

Fig. 13. (a) Echogram (b–d) ADCP velocity and (e–f) MSS profile data over the summit of Sandes showing elevated turbulence coincident with internal wave activity. Time of profile indicated by black vertical marker. The profile was taken in close vicinity to mooring 22.2 as shown in Fig. 3.

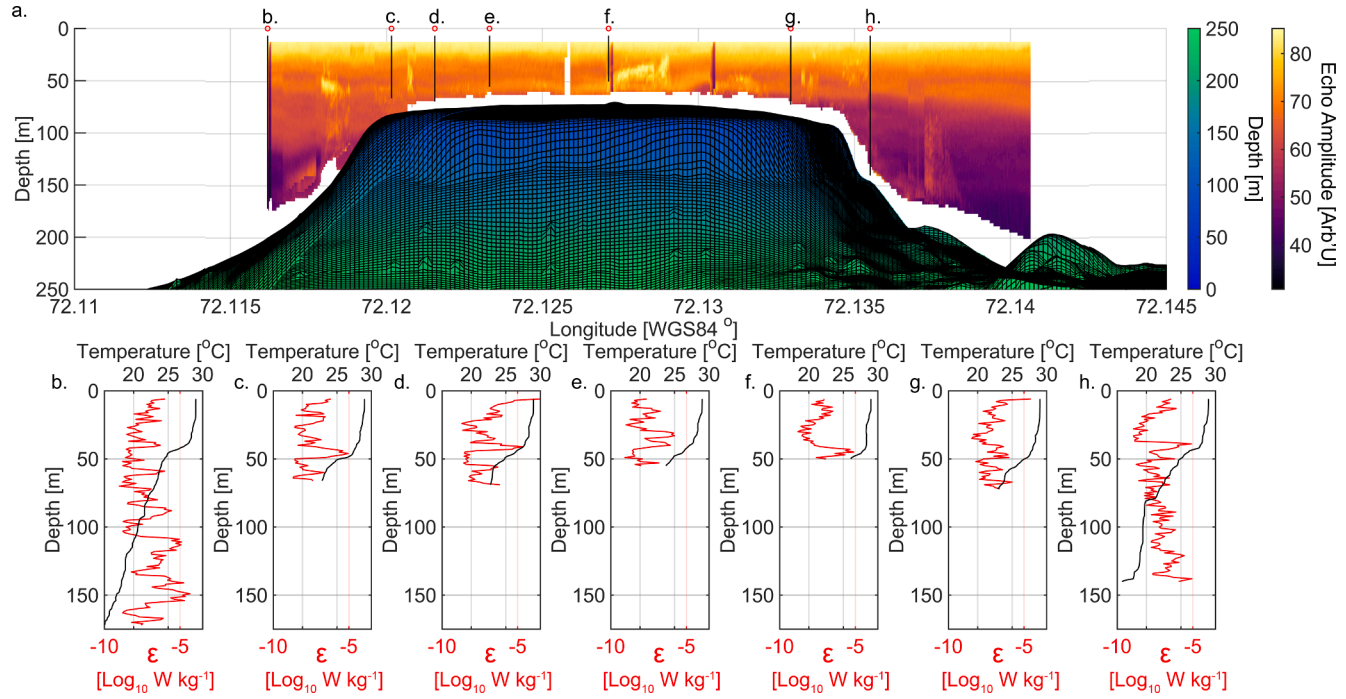

Fig. 14. (a) VMADCP transect of echo amplitude over the summit of sandes overlaid on multibeam bathymetry with the position of mss turbulent kinetic energy dissipation and temperature profiles (b–h) annotated. chronological order of profiles follows east – west.

may generate baroclinic motions that subsequently radiate away from the source region. Because of this, it is highly unlikely that any two seamounts will exhibit identical baroclinic regimes; however, using global estimates of the internal tide (Zhao, 2018), and identifying seamounts that are likely to exhibit amplified internal tides based on background stratification, latitude, and bottom slopes (Robertson et al., 2017), it is feasible to identify sites that may have energetic internal wave regimes with subsequent biological impacts. This does, however, overlook the deficiencies in estimates of global bathymetry what fail to resolve seamounts of the scale presented here.

The importance of physical process in promoting the enhanced biomass and biodiversity which some seamounts exhibit is well

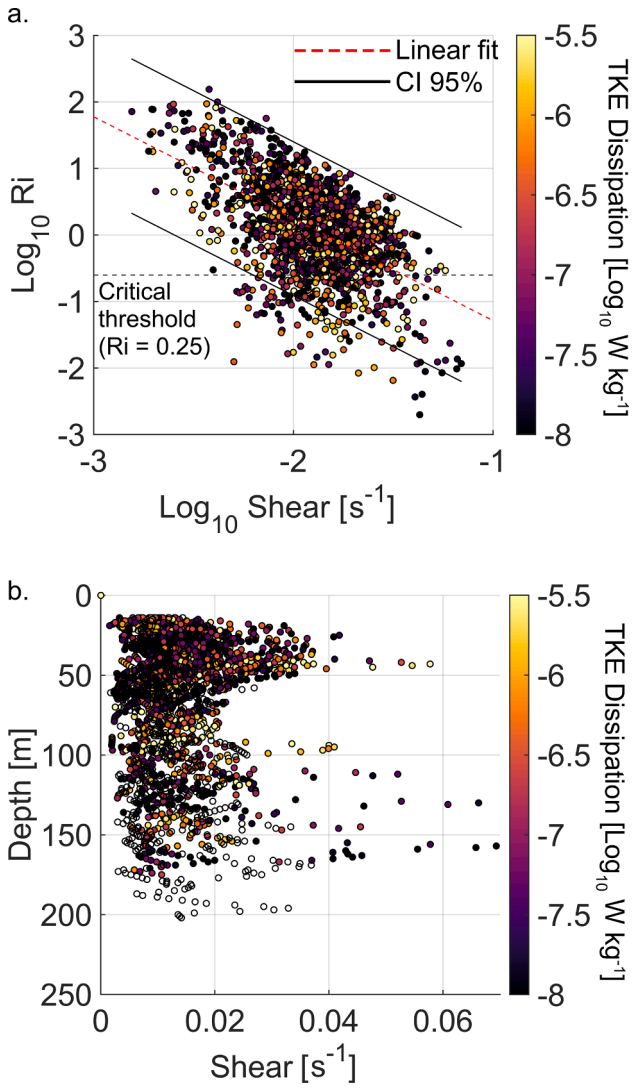

Fig. 15. (a) Ri – Shear relationship from mss profiles and vmadcp data over sandes summit and flanks in 2022. Linear regression fitted, $y = -0.3832x + 0.09045$, $R^2 = 0.298$, with 95 % confidence intervals also shown. (b) Shear with depth from the VMADCP data coinciding with MSS profiles showing elevated shear around the 40 m depth mark. Colouring by TKE dissipation from the corresponding MSS data, points with no colour are shear values deeper than the corresponding TKE profile.

recognised (Pitcher et al., 2008; Roberts et al., 2020; White et al., 2007). Despite this there has been ongoing debate over which processes are the most important in driving the biomass aggregation (Rowden et al., 2010). The picture presented here shows a seamount dominated by high frequency (tidal and higher) energetic, baroclinic dynamics, reinforcing the trend of moving away from slow steady state processes (e.g. Read and Pollard, 2017; Van Haren et al., 2017). Whilst internal waves will act to enhance primary productivity through vertical advection of nutrient rich water (Villamaña et al., 2017), this is less plausible as the driver of high trophic level biomass aggregation over seamounts at the horizontal scale of Sandes due to the absence of retention over the seamount given the lack of Taylor cap formation. Instead internal waves may act as aggregators of zooplankton over and around the summit, boosting secondary productivity (Chen et al., 2021), which given the amplitude of the internal tide at Sandes is a viable mechanism and consistent with the 'halo' of biomass aggregation observed previously around the seamount (Hays et al., 2020).

Overall, our findings suggest the need to change the framework within which these shallow seamount pinnacles are assessed. Assessment of the relationship between physical oceanographic processes, ecosystem functions, and biodiversity, at these features needs to expand to incorporate high-frequency dynamics, as well as the wider background ocean–atmosphere driven conditions. This requires moving away from focusing on single processes towards a more integrated approach. Additionally, it may not be possible in many cases to classify an entire seamount as a single habitat, due to the small spatial scales over which differences in the physical regime are observed.

6. Conclusions

Local dynamics at steep-sloped short horizontal scale seamounts are shown to be driven by high frequency, highly localised dynamics, which are in turn modulated by intra-seasonal basin scale processes. This focus on high frequency processes is a departure from the theory of slow-moving processes (such as Taylor caps) being dominant as was previously posited deeper seamounts.

Within the Indian Ocean, the monsoon and the Indian Ocean dipole modulate the thermocline depth, inducing the variability in the internal wave dynamics at Sandes Seamount. The depth of the thermocline relative to the summit is the primary factor determining the nature of the local physical dynamics, acting as a gating condition of internal wave activity over the summit, potentially with significant ecological impacts over seasonal time scales.

In the presence of IW activity, measured values of turbulence are larger (1×10^{-5} W kg^{-1}) than that of typical values for background open ocean ($1 \times 10^{-8} - 1 \times 10^{-6}$ W kg^{-1}). This strong turbulence is indicative of internal wave generated mixing through shear instability, and is seen most prominently over the flanks, but also co-located with internal wave trains propagating over the summit.

This research highlights the importance of considering these dynamically complex environments from a multi-temporal perspective, with the risk of miss-classification of the local environment based on isolated observations.

Funding sources

Funding for this work was provided by the Garfield Weston Foundation, and Bertarelli Foundation.

CRediT authorship contribution statement

E. Robinson: Writing – review & editing, Writing – original draft, Visualization, Validation, Resources, Methodology, Investigation, Formal analysis, Data curation, Conceptualization. **P. Hosegood:** Writing – review & editing, Writing – original draft, Supervision, Project administration, Methodology, Investigation, Funding acquisition, Data curation, Conceptualization. **A. Bolton:** Visualization, Software, Formal analysis, Data curation.

Declaration of competing interest

The authors declare that they have no known competing financial interests or personal relationships that could have appeared to influence the work reported in this paper.

Data availability

The raw data required to reproduce the above findings cannot be shared at this time as the data also forms part of an ongoing study. The processed data are available from the authors on request.

Acknowledgements

This work was made possible by funding from the Garfield Weston Foundation, and the Bertarelli Foundation, to whom we are grateful for

their support. Additionally, we would like to thank the researchers and crew who joined us onboard the MV Tethys Supporter and lent their assistance with making the fieldwork possible.

Appendix A. Supplementary data

Supplementary data to this article can be found online at https://doi.org/10.1016/j.pocean.2024.103323.

References

Arístegui, J., Mendonça, A., Vilas, J.C., Espino, M., Polo, I., Montero, M.F., Martins, A., 2009. Plankton metabolic balance at two North Atlantic seamounts. Deep Res. Part II Top. Stud. Oceanogr. 56, 2646–2655. https://doi.org/10.1016/j.dsr2.2008.12.025.

Boehlert, G.W., Genin, A., 1987. A review of the effects of seamounts on biological processes. Seamoun. Islands Atolls 43, 319–334. https://doi.org/10.1029/GM043p0319.

Brechner Owens, W., Hogg, N.G., 1980. Oceanic observations of stratified Taylor columns near a bump. Deep Sea Res. Part A Oceanogr. Res. Pap. 27, 1029–1045. https://doi.org/10.1016/0198-0149(80)90063-1.

Burns, J.M., Subrahmanyam, B., 2016. Variability of the seychelles-chagos thermocline ridge dynamics in connection with ENSO and Indian Ocean Dipole. IEEE Geosci. Remote Sens. Lett. 13, 2019–2023. https://doi.org/10.1109/LGRS.2016.2621353.

Campanella, F., Collins, M.A., Young, E.F., Laptikhovsky, V., Whomersley, P., van der Kooij, J., 2021. First insight of meso- and bentho-pelagic fish dynamics around remote seamounts in the south atlantic ocean. Front. Mar. Sci. 8 https://doi.org/10.3389/fmars.2021.663278.

Cascão, I., Domokos, R., Lammers, M.O., Santos, R.S., Silva, M.A., 2019. Seamount effects on the diel vertical migration and spatial structure of micronekton. Prog. Oceanogr. 175, 1–13. https://doi.org/10.1016/j.pocean.2019.03.008.

Chapman, D.C., Haidvogel, D.B., 1992. Formation of taylor caps over a tall isolated seamount in a stratified ocean. Geophys. Astrophys. Fluid Dyn. 64, 31–65. https://doi.org/10.1080/03091929208228084.

Chen, B., Masunaga, E., Smith, S.L., Yamazaki, H., 2021. Diel vertical migration promotes zooplankton horizontal patchiness. J. Oceanogr. 77, 123–135. https://doi.org/10.1007/s10872-020-00564-4.

Clark, M.R., Schlacher, T.A., Rowden, A.A., Stocks, K.I., Consalvey, M., 2012. Science priorities for seamounts: research links to conservation and management. PLoS One 7. https://doi.org/10.1371/journal.pone.0029232.

Dewey, R., Richmond, D., Garrett, C., 2005. Stratified tidal flow over a bump. J. Phys. Oceanogr. 35, 1911–1927. https://doi.org/10.1175/JPO2799.1.

Diaz, C., Foster, N.L., Attrill, M.J., Bolton, A., Ganderton, P., Howell, K.L., Robinson, E., Hosegood, P., 2023. Mesophotic coral bleaching associated with changes in thermocline depth. Nat. Commun. 14, 6528. https://doi.org/10.1038/s41467-023-42279-2.

Domokos, R., 2022. Seamount effects on micronekton at a subtropical central Pacific seamount. Deep. Res. Part I Oceanogr. Res. Pap. 186 https://doi.org/10.1016/j.dsr.2022.103829.

Du, Y., Zhang, Y., Zhang, L.Y., Tozuka, T., Ng, B., Cai, W., 2020. Thermocline warming induced extreme Indian ocean dipole in 2019. Geophys. Res. Lett. 47, 1–10. https://doi.org/10.1029/2020GL090079.

Franks, P.J.S., 1995. Thin layers of phytoplankton: a model of formation by near-inertial wave shear. Deep. Res. Part I 42, 75–91. https://doi.org/10.1016/0967-0637(94)00028-Q.

Franks, P.J.S., Garwood, J.C., Ouimet, M., Cortes, J., Musgrave, R.C., Lucas, A.J., 2020. Stokes drift of plankton in linear internal waves: Cross-shore transport of neutrally buoyant and depth-keeping organisms. Limnol. Oceanogr. 65, 1286–1296. https://doi.org/10.1002/lno.11389.

Galbraith, G.F., Cresswell, B.J., McCormick, M.I., Bridge, T.C., Jones, G.P., 2022. Contrasting hydrodynamic regimes of submerged pinnacle and emergent coral reefs. PLoS One 17, 1–26. https://doi.org/10.1371/journal.pone.0273092.

Garrett, C., Kunze, E., 2007. Internal tide generation in the deep ocean. Annu. Rev. Fluid Mech. 39, 57–87. https://doi.org/10.1146/annurev.fluid.39.050905.110227.

Genin, A., 2004. Bio-physical coupling in the formation of zooplankton and fish aggregations over abrupt topographies. J. Mar. Syst. 50, 3–20. https://doi.org/10.1016/j.jmarsys.2003.10.008.

Hall, R.A., Huthnance, J.M., Williams, R.G., 2013. Internal wave reflection on shelf slopes with depth-varying stratification. J. Phys. Oceanogr. 43, 248–258. https://doi.org/10.1175/JPO-D-11-0192.1.

Hamann, M.M., Alford, M.H., Lucas, A.J., Waterhouse, A.F., Voet, G., 2020. Turbulence driven by reflected internal tides in a supercritical submarine canyon. J. Phys. Oceanogr. 51, 591–609. https://doi.org/10.1175/jpo-d-20-0123.1.

Harris, P.T., 2007. Applications of geophysical information to the design of a representative system of marine protected areas in southeastern Australia. Spec. Pap. - Geol. Assoc. Canada 463–482.

Hays, G.C., Koldewey, H.J., Andrzejaczek, S., Attrill, M.J., Barley, S., Bayley, D.T.I., Benkwitt, C.E., Block, B., Schallert, R.J., Carlisle, A.B., Carr, P., Chapple, T.K., Collins, C., Diaz, C., Dunn, N., Dunbar, R.B., Eager, D.S., Engel, J., Embling, C.B., Esteban, N., Ferretti, F., Foster, N.L., Freeman, R., Gollock, M., Graham, N.A.J., Harris, J.L., Head, C.E.I., Hosegood, P., Howell, K.L., Hussey, N.E., Jacoby, D.M.P., Jones, R., Sannassy Pilly, S., Lange, I.D., Letessier, T.B., Levy, E., Lindhart, M., McDevitt-Irwin, J.M., Meekan, M., Meeuwig, J.J., Micheli, F., Mogg, A.O.M., Mortimer, J.A., Mucciarone, D.A., Nicoll, M.A., Nuno, A., Perry, C.T., Preston, S.G., Rattray, A.J., Robinson, E., Roche, R.C., Schiele, M., Sheehan, E.V., Sheppard, A., Sheppard, C., Smith, A.L., Soule, B., Spalding, M., Stevens, G.M.W., Steyaert, M., Stiffel, S., Taylor, B.M., Tickler, D., Trevail, A.M., Trueba, P., Turner, J., Votier, S., Wilson, B., Williams, G.J., Williamson, B.J., Williamson, M.J., Wood, H., Curnick, D. J., 2020. A review of a decade of lessons from one of the world's largest MPAs: conservation gains and key challenges. Mar. Biol. 167, 1–22. https://doi.org/10.1007/s00227-020-03776-w.

Holloway, P.E., Merrifield, M.A., 1999. Internal tide generation by seamounts, ridges, and islands. J. Geophys. Res. Ocean. 104, 25937–25951. https://doi.org/10.1029/1999jc900207.

Hosegood, P.J., Nimmo-Smith, W.A.M., Proud, R., Adams, K., Brierley, A.S., 2019. Internal lee waves and baroclinic bores over a tropical seamount shark 'hot-spot'. Prog. Oceanogr. 172, 34–50. https://doi.org/10.1016/j.pocean.2019.01.010.

Huppert, H.E., 1975. Some remarks on the initiation of inertial Taylor columns. J. Fluid Mech. 67, 397–412. https://doi.org/10.1017/S0022112075000377.

International Hydrographic Organization, 2019. Standardization of Undersea Feature Names. IHO B-6.

Johnston, S., Merrifield, M.A., 2003. Internal tide scattering at seamounts, ridges, and islands. J. Geophys. Res. Ocean. 108, 1–17. https://doi.org/10.1029/2002JC001528.

Klymak, J.M., Legg, S., Pinkel, R., 2010. High-mode stationary waves in stratified flow over large obstacles. J. Fluid Mech. 644, 321–336. https://doi.org/10.1017/S0022112009992503.

Lamb, K.G., 2014. Internal wave breaking and dissipation mechanisms on the continental slope/shelf. Annu. Rev. Fluid Mech. 46, 231–254. https://doi.org/10.1146/annurev-fluid-011212-140701.

Lavelle, J.W., Mohn, C., 2010. Motion, commotion, and biophysical connections at deep ocean seamounts. Oceanography 23, 90–103. https://doi.org/10.5670/oceanog.2010.64.

LeBlond, P.H., Mysak, L.A., 1978. Waves in the ocean. Elsevier Oceanography Series.

Legg, S., 2021. Mixing by oceanic lee waves. Annu. Rev. Fluid Mech. 53, 173–201. https://doi.org/10.1146/annurev-fluid-051220-043904.

Lennert-Cody, C.E., Franks, P.J.S., 1999. Plankton patchiness in high-frequency internal waves. Mar. Ecol. Prog. Ser. 186, 59–66. https://doi.org/10.3354/meps186059.

Lennert-Cody, C.E., Franks, P.J.S., 2002. Fluorescence patches in high-frequency internal waves. Mar. Ecol. Prog. Ser. 235, 29–42. https://doi.org/10.3354/meps235029.

Liu, H., Duan, Y., Yan, X., Pang, C., 2022. Interannual variability of the thermocline depth in the south-central Indian Ocean: Respective influences of IOD and ENSO. Int. J. Climatol. 42, 5111–5120. https://doi.org/10.1002/joc.7522.

Lu, B., Ren, H.L., 2020. What caused the extreme indian ocean dipole event in 2019? Geophys. Res. Lett. 47 https://doi.org/10.1029/2020GL087768.

Ma, J., Song, J., Li, X., Wang, Q., Zhong, G., 2021. Multidisciplinary indicators for confirming the existence and ecological effects of a Taylor column in the Tropical Western Pacific Ocean. Ecol. Indic. 127, 107777 https://doi.org/10.1016/j.ecolind.2021.107777.

McClain, C.R., 2007. Seamounts: Identity crisis or split personality? J. Biogeogr. 34, 2001–2008. https://doi.org/10.1111/j.1365-2699.2007.01783.x.

Mohn, C., White, M., Denda, A., Erofeeva, S., Springer, B., Turnewitsch, R., Christiansen, B., 2021. Dynamics of currents and biological scattering layers around Senghor Seamount, a shallow seamount inside a tropical Northeast Atlantic eddy corridor. Deep. Res. Part I Oceanogr. Res. Pap. 171, 103497 https://doi.org/10.1016/j.dsr.2021.103497.

Morato, T., Hoyle, S.D., Allain, V., Nicol, S.J., 2010. Seamounts are hotspots of pelagic biodiversity in the open ocean. Proc. Natl. Acad. Sci. u. s. a. 107, 9707–9711. https://doi.org/10.1073/pnas.0910290107.

Mouriño, B., Fernández, E., Serret, P., Harbour, D., Sinha, B., Pingree, R., 2001. Variability and seasonality of physical and biological fields at the Great Meteor Tablemount (subtropical NE Atlantic). Oceanol. Acta 24, 167–185. https://doi.org/10.1016/S0399-1784(00)01138-5.

Müller, M., Cherniawsky, J.Y., Foreman, M.G.G., von Storch, J.-S., 2012. Global M 2 internal tide and its seasonal variability from high resolution ocean circulation and tide modeling. Geophys. Res. Lett. 39, 1–6. https://doi.org/10.1029/2012GL053320.

NOAA, 2023. Dipole Mode Index Timeseries [WWW Document]. URL https://psl.noaa.gov/gcos_wgsp/Timeseries/DMI/.

Oakey, N.S., 1982. Determination of the rate of dissipation of turbulent energy from simultaneous temperature and velocity shear microstructure measurements. J. Phys. Oceanogr. 12, 256–271. https://doi.org/10.1175/1520-0485(1982)012<0256:DOTROD>2.0.CO;2.

Parker, B.N.O., A.A., 2007. Tidal Analysis and Prediction: Noaa Special Publication Nos Co-Ops 3. National Oceanic and Atmospheric Administration.

Pitcher, T.J., Morato, T., Hart, P.J.B., Clark, M.R., Haggan, N., Santos, R.S., 2008. Seamounts: Ecology, Fisheries & Conservation, Seamounts: Ecology, Fisheries & Conservation. Doi: 10.1002/9780470691953.

Read, J., Pollard, R., 2017. An introduction to the physical oceanography of six seamounts in the southwest Indian Ocean. Deep. Res. Part II Top. Stud. Oceanogr. 136, 44–58. https://doi.org/10.1016/j.dsr2.2015.06.022.

Reid, E.C., DeCarlo, T.M., Cohen, A.L., Wong, G.T.F., Lentz, S.J., Safaie, A., Hall, A., Davis, K.A., 2019. Internal waves influence the thermal and nutrient environment on a shallow coral reef. Limnol. Oceanogr. 64, 1949–1965. https://doi.org/10.1002/lno.11162.

Roberts, M.J., Ternon, J.F., Marsac, F., Noyon, M., Payne, A.I.L., 2020. The MADRidge project: Bio-physical coupling around three shallow seamounts in the South West Indian Ocean. Deep. Res. Part II Top. Stud. Oceanogr. 176, 104813 https://doi.org/10.1016/j.dsr2.2020.104813.

Robertson, R., Dong, J., Hartlipp, P., 2017. Diurnal critical latitude and the latitude dependence of internal tides, internal waves, and mixing based on barcoo seamount. J. Geophys. Res. Ocean. 122, 7838–7866. https://doi.org/10.1002/2016JC012591.

Robinson, E., Hosegood, P., Bolton, A., 2023. Dynamical oceanographic processes impact on reef manta ray behaviour: Extreme Indian Ocean Dipole influence on local internal wave dynamics at a remote tropical atoll. Prog. Oceanogr. 218, 103129 https://doi.org/10.1016/j.pocean.2023.103129.

Rowden, A.A., Dower, J.F., Schlacher, T.A., Consalvey, M., Clark, M.R., 2010. Paradigms in seamount ecology: Fact, fiction and future. Mar. Ecol. 31, 226–241. https://doi.org/10.1111/j.1439-0485.2010.00400.x.

Saji, N.H., Goswami, B.N., Vinayachandran, P.N., Yamagata, T., 1999. A dipole mode in the tropical Indian Ocean. Nature 401, 360–363. https://doi.org/10.1038/43854.

Santos, M., Moita, M.T., Bashmachnikov, I., Menezes, G.M., Carmo, V., Loureiro, C.M., Mendonça, A., Silva, A.F., Martins, A., 2013. Phytoplankton variability and oceanographic conditions at Condor seamount, Azores (NE Atlantic). Deep. Res. Part II Top. Stud. Oceanogr. 98, 52–62. https://doi.org/10.1016/j.dsr2.2013.05.037.

Shriver, J.F., Arbic, B.K., Richman, J.G., Ray, R.D., Metzger, E.J., Wallcraft, A.J., Timko, P.G., 2012. An evaluation of the barotropic and internal tides in a high-resolution global ocean circulation model. J. Geophys. Res. Ocean. 117 https://doi.org/10.1029/2012JC008170.

Stashchuk, N., Vlasenko, V., 2021. Internal wave dynamics over isolated seamount and its influence on coral larvae dispersion. Front. Mar. Sci. 8 https://doi.org/10.3389/fmars.2021.735358.

Staudigel, H., Koppers, A., Lavelle, J.W., Pitcher, T., Shank, T., 2010. Defining the Word "Seamount". Oceanography 23, 20–21. https://doi.org/10.5670/oceanog.2010.85.

Stevens, C., Consalvey, M., Devine, J., Clark, M., 2014. Mixing and transport near the shallow-crested Rumble III seamount and the implications for plankton distribution. New Zeal. J. Mar. Freshw. Res. 48, 194–215. https://doi.org/10.1080/00288330.2013.872154.

Tanaka, M., Genin, A., Endo, Y., Ivey, G.N., Yamazaki, H., 2021. The potential role of turbulence in modulating the migration of demersal zooplankton. Limnol. Oceanogr. 66, 855–864. https://doi.org/10.1002/lno.11646.

Toole, J.M., Schmitt, R.W., Polzin, K.L., Kunze, E., 1997. Near-boundary mixing above the flanks of a midlatitude seamount. J. Geophys. Res. Ocean. 102, 947–959. https://doi.org/10.1029/96jc03160.

Trasviña-Castro, A., Gutierrez De Velasco, G., Valle-Levinson, A., González-Armas, R., Muhlia, A., Cosio, M.A., 2003. Hydrographic observations of the flow in the vicinity of a shallow seamount top in the Gulf of California. Estuar. Coast. Shelf Sci. 57, 149–162. https://doi.org/10.1016/S0272-7714(02)00338-4.

Turnewitsch, R., Dumont, M., Kiriakoulakis, K., Legg, S., Mohn, C., Peine, F., Wolff, G., 2016. Progress in Oceanography Tidal influence on particulate organic carbon export fluxes around a tall seamount. Prog. Oceanogr. 149, 189–213. https://doi.org/10.1016/j.pocean.2016.10.009.

van Haren, H., 2023. Internal tidal sloshing and a non-linear wave source away from topography. Deep Sea Res. Part I Oceanogr. Res. Pap. 196, 104021 https://doi.org/10.1016/j.dsr.2023.104021.

Van Haren, H., Hanz, U., de Stigter, H., Mienis, F., Duineveld, G., 2017. Internal wave turbulence at a biologically rich Mid-Atlantic seamount. PLoS One 12, 1–16. https://doi.org/10.1371/journal.pone.0189720.

Van Haren, H., Duineveld, G., Mienis, F., 2019. Internal wave observations off Saba Bank. Front. Mar. Sci. 5, 1–13. https://doi.org/10.3389/fmars.2018.00528.

Villamaña, M., Mouriño-Carballido, B., Marañón, E., Cermeño, P., Chouciño, P., da Silva, J.C.B., Díaz, P.A., Fernández-Castro, B., Gilcoto, M., Graña, R., Latasa, M., Magalhaes, J.M., Luis Otero-Ferrer, J., Reguera, B., Scharek, R., 2017. Role of internal waves on mixing, nutrient supply and phytoplankton community structure during spring and neap tides in the upwelling ecosystem of Ría de Vigo (NW Iberian Peninsula). Limnol. Oceanogr. 62, 1014–1030. https://doi.org/10.1002/lno.10482.

Watling, L., Auster, P.J., 2017. Seamounts on the high seas should be managed as vulnerable marine ecosystems. Front. Mar. Sci. 4, 1–4. https://doi.org/10.3389/fmars.2017.00014.

White, M., Bashmachnikov, I., Arstegui, J., Martins, A., 2007. Physical processes and seamount productivity. In: Seamounts: ecology, fisheries & conservation. Blackwell Publishing Ltd, Oxford, UK, pp. 62–84. https://doi.org/10.1002/9780470691953.ch4.

Wyatt, A.S.J., Leichter, J.J., Toth, L.T., Miyajima, T., Aronson, R.B., Nagata, T., 2020. Heat accumulation on coral reefs mitigated by internal waves. Nat. Geosci. 13, 28–34. https://doi.org/10.1038/s41561-019-0486-4.

Yesson, C., Clark, M.R., Taylor, M.L., Rogers, A.D., 2011. The global distribution of seamounts based on 30 arc seconds bathymetry data. Deep Res. Part I Oceanogr. Res. Pap. 58, 442–453. https://doi.org/10.1016/j.dsr.2011.02.004.

Yesson, C., Letessier, T.B., Nimmo-Smith, A., Hosegood, P., Brierley, A.S., Hardouin, M., Proud, R., 2020. List of Seamounts in the World Oceans - an Update. https://doi.org/10.1594/PANGAEA.921688.

Zhang, L., Buijsman, M.C., Comino, E., Swinney, H.L., 2017. Internal wave generation by tidal flow over periodically and randomly distributed seamounts. J. Geophys. Res. Ocean. 122, 5063–5074. https://doi.org/10.1002/2017JC012884.

Zhao, Z., 2018. The global mode-2 M2 internal tide. J. Geophys. Res. Ocean. 123, 7725–7746. https://doi.org/10.1029/2018JC014475.